

Amortized Molecular Optimization via Group Relative Policy Optimization

Muhammad bin Javaid*¹ Hasham Hussain*^{1,2} Ashima Khanna^{3,4} Berke Kişin¹ Jonathan Pirnay^{3,4}
Alexander Mitsos⁵ Dominik G. Grimm^{3,4} Martin Grohe¹

Abstract

Molecular design encompasses tasks ranging from *de-novo* design to structural alteration of given molecules or fragments. For the latter, state-of-the-art methods predominantly function as “Instance Optimizers”, expending significant compute restarting the search for every input structure. While model-based approaches theoretically offer amortized efficiency by learning a policy transferable to unseen structures, existing methods struggle to generalize. We identify a key failure mode: the high variance arising from the heterogeneous difficulty of distinct starting structures. To address this, we introduce GRXForm, adapting a pre-trained Graph Transformer model that optimizes molecules via sequential atom-and-bond additions. We employ Group Relative Policy Optimization (GRPO) for goal-directed fine-tuning to mitigate variance by normalizing rewards relative to the starting structure. Empirically, GRXForm generalizes to out-of-distribution molecular scaffolds without inference-time oracle calls or refinement, achieving scores in multi-objective optimization competitive with leading instance optimizers.

1. Introduction

The potential of generative AI for molecular design lies in its ability to aid in discovery, applying learned chemi-

*Equal contribution

¹RWTH Aachen University, Department of Computer Science, Ahornstrasse 55, 52074 Aachen, Germany ²Alfred E. Tiefenbacher (GmbH & Co. KG), Van-der-Smissen-Strasse 1, 22767 Hamburg, Germany ³Technical University of Munich, TUM Campus Straubing for Biotechnology and Sustainability, Bioinformatics, Petersgasse 18, 94315 Straubing, Germany ⁴University of Applied Sciences Weihenstephan-Triesdorf, Bioinformatics, Petersgasse 18, 94315 Straubing, Germany ⁵RWTH Aachen University, Process Systems Engineering (AVT.SVT), Forckenbeckstrasse 51, 52074 Aachen, Germany. Correspondence to: Muhammad bin Javaid <javaid@informatik.rwth-aachen.de>.

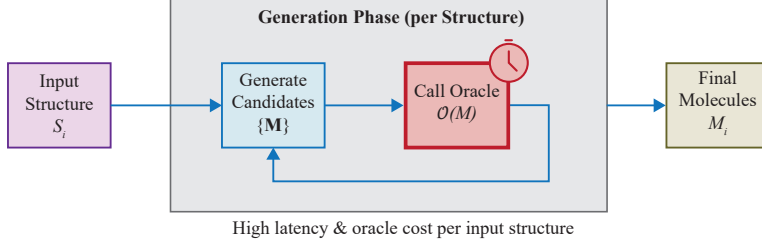
Code available at: github.com/Hash-hh/GRXForm
Preprint. February 13, 2026.

cal principles to rapidly propose structural modifications that optimize specific target properties for any given input molecular structure. Ideally, such a system would perform tasks such as scaffold decoration, linker design, and lead optimization in a single forward pass, thereby amortizing the search cost over the training period.

However, recent progress has heavily favored **instance-specific optimization**. Leading methods, such as Genetic Algorithms (GAs) (Tripp & Hernández-Lobato, 2023; Kim et al., 2024) and guided Discrete Diffusion (Lee et al., 2025), excel at deep search: by expending thousands of queries to an external scoring function or simulation (an “oracle”) for each distinct design task, they navigate complex landscapes to find highly optimized solutions. While invaluable in scenarios such as late-stage lead optimization in drug design (Hughes et al., 2011), where the computational cost per molecule is justified, this paradigm is prohibitive for high-throughput tasks. For scenarios requiring the rapid elaboration of entire chemical libraries or dynamic user-in-the-loop design, relying on an expensive iterative search for every single entry creates a significant scalability bottleneck.

The scalability limitations of instance optimization are often less apparent in tasks relying on computationally trivial proxy oracles, such as Quantitative Estimate of Drug-likeness (QED) (Bickerton et al., 2012) and LogP (lipophilicity) (Wildman & Crippen, 1999). Because such heuristic functions execute in milliseconds, they obscure the cost of iterative search methods. The *Practical Molecular Optimization* (PMO) benchmark (Gao et al., 2022) represented a significant step forward by imposing a strict budget of 10,000 oracle calls per task to penalize sample inefficiency. However, this framework remains confined to evaluating the efficiency of solving isolated tasks from scratch, neglecting the cumulative efficiency gains of amortization in dynamic design settings, where a single learned policy can instantly generalize to thousands of diverse structural constraints as needed. While a 10^4 budget is feasible for analytical functions, for high-fidelity oracles like protein-ligand docking (minutes per call) or free energy perturbation (hours per call), a method requiring 10^4 evaluations per molecule is computationally prohibitive; even more so since it must be repeated whenever a new structural constraint is added to the design task.

A. Search-Based / Instance Optimization



B. Amortized Optimization

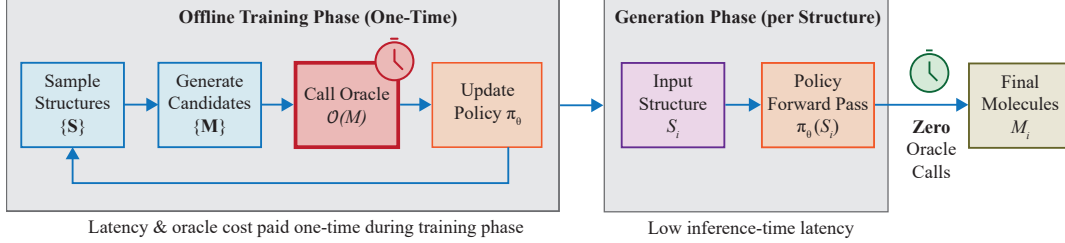


Figure 1. Comparison of optimization paradigms. **(A) Instance Optimization:** Requires an expensive iterative search with thousands of oracle calls for every new input structure S_i , resulting in high cost that scales linearly with library size. **(B) Amortized Optimization:** Front-loads computation into offline training. The learned policy π_θ generates optimized molecules for new, unseen inputs S_i in a single forward pass without inference-time oracle calls, enabling scalable, high-throughput design.

We argue that, in order for generative models to be scalable to high-fidelity oracles when performing dynamic design with user-input constraints or elaborating chemical libraries, we must prioritize **amortized optimization**. Here, the goal is to learn a robust conditional policy $\pi_\theta(y|x)$, that, once trained, can generate high-quality modifications y for a starting molecular structure x with no inference-time oracle calls required.

Historically, amortized reinforcement learning (RL) for molecules has struggled to match the peak performance of exhaustive, search-based methods (Jensen, 2019; Gao et al., 2022; Tripp & Hernández-Lobato, 2023). Bridging this gap requires learning a policy capable of generalizing across a vast and discontinuous chemical space. Moreover, real-world drug discovery is inherently a multi-objective problem, requiring the simultaneous optimization of conflicting properties (e.g., maximizing potency while maintaining solubility). This further complicates the exploration of rugged, non-convex landscapes, as improvements in one dimension often inevitably degrade performance in another. This task is further complicated by the variance in conditional difficulty. For example, varying the starting scaffold (the fixed molecular core used as the initial state) can dramatically shift the expected reward landscape. Some structures easily yield high-scoring derivatives, while others reside in chemically constrained regions. Standard RL algorithms can struggle to normalize these disparate signals effectively, leading to high-variance gradient estimates where the learning signal is dominated by “easy” instances rather than

difficult optimization improvements.

To address these challenges, we present GRXForm (Group **R**elative **X**former), which builds upon the GraphXForm architecture (Pirnay et al., 2025) and parametrizes a step-wise, atom-by-atom constructive policy. As in the original architecture, this policy is implemented using a Graph Transformer with valence-based action masking to ensure compliance with chemical validity rules. The GraphXForm framework relies on a self-improvement loop to mimic trajectories found by a search heuristic. In contrast, to stabilize the training process across diverse input structures, we adapted Group Relative Policy Optimization (GRPO) (Shao et al., 2024), originally introduced for training Large Language Model reasoning, to the molecular domain. Instead of estimating a global baseline, GRPO samples a group of G distinct completed trajectories from each starting structure and normalizes rewards relative to the group mean. This effectively creates a dynamic baseline. Even if a starting molecular structure is difficult to optimize and all trajectories yield low raw scores, GRPO identifies and rewards the *relatively* best attempt. We demonstrate that this formulation is essential to mitigate the high-variance reward landscape caused by heterogeneous task difficulty, which is known to destabilize standard reinforcement learning (Rennie et al., 2017; Shao et al., 2024).

By effectively stabilizing the training process, we propose a purely amortized framework that achieves strong optimization performance without any inference-time oracle calls.

This framework bridges the gap between fast generation and high-scoring search methods. We demonstrate that GRX-Form generalizes to unseen starting molecular structures and effectively scales to multi-objective settings. Moreover, despite its flexibility, our method remains competitive with the current top-performing instance optimizers on the PMO benchmark, a fundamental instance optimization test.

2. Related Work

We classify generative molecular design methods into the two aforementioned distinct paradigms: instance optimization and amortized optimization. Appendix A provides a comprehensive taxonomy and a detailed survey of existing approaches, identifying which paradigm they fall under.

2.1. Instance Optimization

Methods in this category rely on external scoring functions to guide a traversal of chemical space during inference. Evolutionary strategies, such as Mol GA (Tripp & Hernández-Lobato, 2023), evolve a population of molecular graphs through mutation and crossover operations. While Mol GA serves as a formidable baseline on the PMO benchmark (Gao et al., 2022), it incurs a high inference-time cost, typically requiring thousands of oracle evaluations per instance to effectively navigate the chemical space. Similarly, state-of-the-art models for goal-directed generation like the discrete diffusion model GenMol (Lee et al., 2025) effectively function as instance optimizers. Although GenMol utilizes a generalist denoiser, it relies on an iterative “fragment remasking” loop, functionally equivalent to Gibbs sampling, to optimize properties. This dependence on active inference-time search prevents single-pass optimization.

2.2. Amortized Optimization

Amortized methods learn a conditional policy $\pi_\theta(y|x)$ to generate optimized structures directly, eliminating the need for extensive search at test time. To ensure chemical validity, frameworks like LibINVENT (within REINVENT 4) (Loeffler et al., 2024) employ penalty-based regularization anchored to a pre-trained prior. While effective for validity, this regularization actively resists the policy drift required to reach high-reward regions far from the training distribution. Conditional encoder-decoder models, such as DrugEx v3 (Liu et al., 2023), address this by training a Graph Transformer via multi-objective REINFORCE. To manage the high variance of policy gradients, DrugEx v3 relies on a fixed exploration network and Pareto-based ranking for multi-objective optimization.

Recently, self-improvement approaches have been proposed, notably GraphXForm (Pirnay et al., 2025), which trains a policy to imitate step-wise molecular generation action

trajectories discovered by the “Take a Step and Reconsider” (TASAR) algorithm (Pirnay & Grimm, 2024b). TASAR functions as a decoding search heuristic that utilizes the current policy to guide Stochastic Beam Search (Kool et al., 2019), necessitating frequent oracle calls to evaluate all candidate leaves across multiple search steps. The resulting best-scoring trajectories (molecules) are aggregated in a replay buffer for the policy to imitate; consequently, while the resulting policy is technically amortized, the training process is computationally intensive due to the reliance on this oracle-dependent search to generate supervision.

In contrast, GRXForm circumvents the reliance on auxiliary exploration networks or restrictive priors. By relying on the stepwise action masking of the underlying GraphX-Form architecture to enforce chemical validity, we bypass the need for prior-based regularization in the loss function. Furthermore, we employ GRPO to normalize rewards with per-starting structure baselines, stabilizing the learning of a policy that generalizes effectively across diverse molecular structures.

3. Methodology

3.1. Structurally Constrained Generation

In molecular design tasks, purely *de-novo* design is often less practical than design under structural constraints, where specific substructures must be preserved. These tasks encompass a range of objectives (Hughes et al., 2011; Noutahi et al., 2024): **scaffold decoration**, where the fixed core structure (comprising ring systems and linkers) is preserved while the agent attaches functional groups or side chains; **motif extension**, which involves extending a small structural fragment into a larger, complete molecular graph; and **superstructure generation**, where the agent must generate a molecule containing a specific input substructure. Additional constrained tasks include **linker design**, requiring the generation of a bridge to connect two or more disjoint fragments; **lead optimization**, in which a high-affinity molecule is modified to improve desired properties; and **scaffold morphing**, where the core scaffold structure itself is modified (e.g., via ring expansion) while retaining specific substituent patterns.

In our framework, we treat these tasks uniformly: the generation process initiates from a non-empty subgraph s_0 (the scaffold or fragment), and the policy π sequentially adds atoms and bonds to elaborate this structure. Furthermore, by simply initializing s_0 as a single atom, our framework seamlessly encompasses *de-novo* generation.

We formulate amortized molecular optimization as learning a conditional policy π_θ that sequentially constructs a molecular graph G . The goal is to maximize a scalar reward $R(G)$ derived from an external oracle (e.g., a property predictor

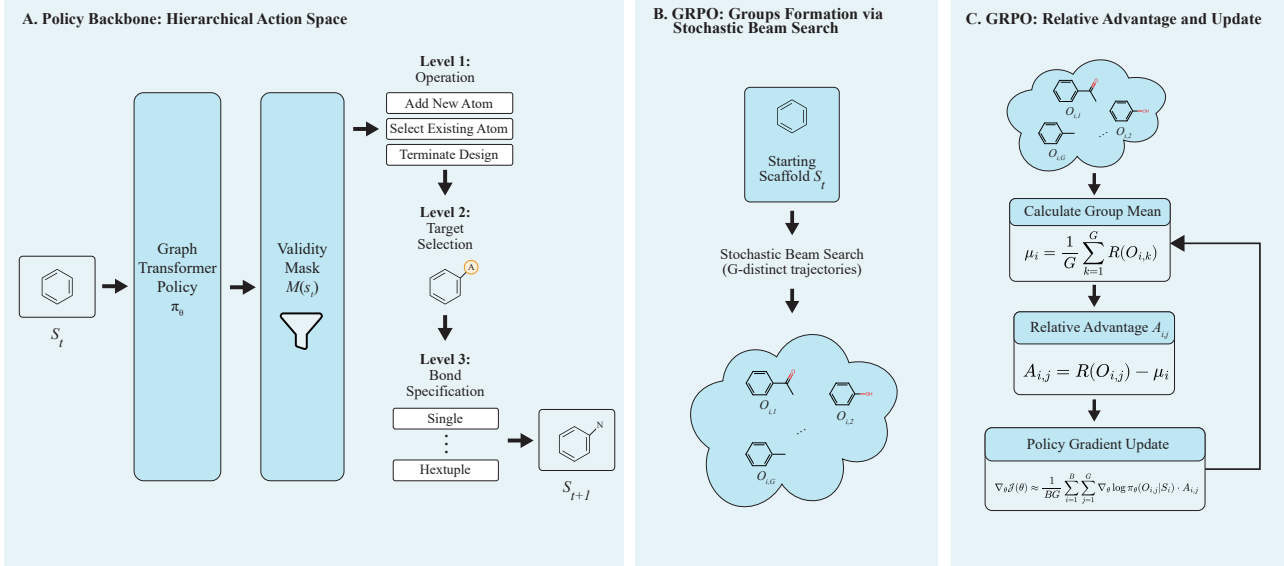


Figure 2. Overview of the GRXForm policy architecture and training mechanism.

or docking simulation) that evaluates the desirability of the generated structure.

3.2. Policy Architecture

To implement the conditional policy $\pi_\theta(y|x)$, we adopt the architecture, action space, and pre-training of GraphXForm (Pirnay et al., 2025) as our structural backbone. The model architecture is a decoder-only Graph Transformer, which operates directly on the molecular graph representation. However, unlike the original framework which utilizes self-improvement learning (Pirnay & Grimm, 2024a), we propose a direct on-policy RL approach built upon GRPO (Shao et al., 2024). We provide a schematic overview of the hierarchical action space and training mechanism in Figure 2.

Action Space. To handle the discrete nature of molecule generation, the model constructs the graph via a sequential Markov Decision Process. At each step t , the policy samples a composite action decomposed into three hierarchical levels: (1) *Operation Selection* (Add Atom, Modify Existing, or Stop), (2) *Target Selection* (Where to connect), and (3) *Bond Specification* (Bond order). A validity mask $M(s_t)$ is applied at each step to strictly enforce valence constraints, masking any actions that would violate basic atomic valency rules, thus ensuring that all generated structures are chemically valid by construction.

Initialization. Prior to RL fine-tuning, the model is pre-trained on the ChEMBL database (version 35) (Davies et al., 2015) via supervised teacher forcing. We distinguish here between *chemical validity* and *plausibility*: while our action

masking strictly enforces valence rules (validity), not all topologically valid graphs correspond to stable or realistic molecules. Pre-training imparts a prior of chemical plausibility, biasing the policy’s initial distribution to resemble the manifold of real-world, synthesizable chemistry rather than merely randomly assembled valid atoms.

We refer the reader to Appendix B for a detailed breakdown of the action space decomposition, the model architecture including the attention mechanisms, and the pre-training.

3.3. Group Relative Policy Optimization (GRPO)

A key contribution is the adaptation of GRPO to the domain of constrained molecular design. Standard RL methods often struggle in this domain due to the high variance in conditional difficulty.

The Variance Problem. In constrained generation, the difficulty of the optimization task is heavily dependent on the starting structure s_0 . For example, in scaffold decoration tasks, some scaffolds are “easy” (chemically permissible to extensive modification), while others are “hard” (constrained by sterics or valency) to optimize for a given property. A global baseline (as used in standard REINFORCE) fails to account for this: a mediocre score on a hard scaffold might actually represent a high-quality policy decision, while a high score on an easy scaffold might be trivial. Figure 3 visualizes this problem.

Group Formation. To resolve this, GRPO eliminates the need for a critic value network by normalizing rewards relative to a group of trajectories sampled from the *same* starting structure. Formally, for each training step, we sam-

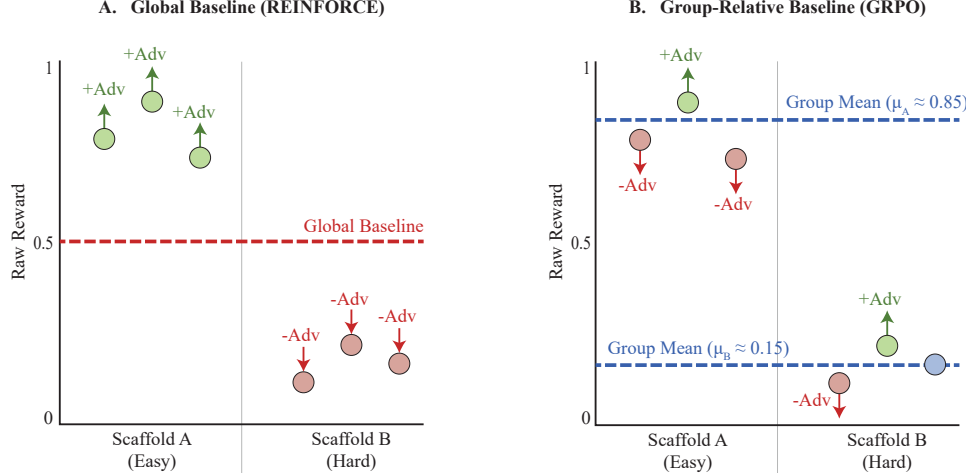


Figure 3. Comparison of advantage estimation strategies. (A) **Global Baseline (REINFORCE)** fails to account for heterogeneous scaffold difficulty, leading to biased gradients. (B) **Group-Relative Baseline (GRPO)** uses instance-specific group means (μ_A, μ_B) to normalize rewards, stabilizing the learning signal across both easy and hard tasks.

ple a batch of B starting molecular structures $\{S_1, \dots, S_B\}$. For each structure S_i , we generate a group of G distinct molecular completions $\{O_{i,1}, \dots, O_{i,G}\}$. To form these groups, we use Stochastic Beam Search (SBS) (Kool et al., 2019), adopting the decoding strategy native to the GraphX-Form architecture (Pirnay et al., 2025). Unlike independent sampling (which can suffer from mode collapse, producing similar high-probability trajectories), SBS guarantees that the G sampled action sequences are diverse while still following the high-probability regions of the policy. This diversity helps ensure sufficient variance within the group to calculate meaningful relative advantages.

Relative Advantage and Update. We adopt the Dr. GRPO formulation (Liu et al., 2025), which modifies the standard GRPO advantage calculation to eliminate specific optimization biases. First, we drop the division by the group standard deviation to avoid *question-level difficulty bias*, where tasks with low variance (e.g., trivially easy or impossible scaffolds) are disproportionately overweighted in the gradient update. Second, we remove the normalization by trajectory length to prevent *length bias*, which otherwise penalizes concise correct solutions. Consequently, we compute the advantage $A_{i,j}$ solely by centering the reward $R(O_{i,j})$ against the group mean:

$$A_{i,j} = R(O_{i,j}) - \mu_i \quad (1)$$

where $\mu_i = \frac{1}{G} \sum_{k=1}^G R(O_{i,k})$ is the mean reward of the group sampled from starting structure S_i .

Furthermore, as sampling trajectories is inexpensive compared to updating the policy parameters θ , we perform only a single gradient update per batch of sampled trajectories. As a result, the standard PPO-style clipping mechanism

Algorithm 1 GRXForm Training Loop

```

1: Input: Set of starting structures  $\mathcal{D}$ , Reward oracle  $R$ , Initial policy  $\pi_\theta$ 
2: Hyperparameters: Batch size  $B$ , Group size  $G$ , Learning rate  $\alpha$ 
3: repeat
4:   Sample batch of starting structures  $\{S_1, \dots, S_B\} \sim \mathcal{D}$ 
5:   Initialize gradient accumulator  $\Delta\theta \leftarrow 0$ 
6:   for  $i = 1$  to  $B$  do
7:     Generate group  $\mathcal{O}_i = \{O_{i,1}, \dots, O_{i,G}\}$  using SBS on  $\pi_\theta(\cdot | S_i)$ 
8:     Compute rewards  $r_{i,j} \leftarrow R(O_{i,j})$  for all  $j \in \{1, \dots, G\}$ 
9:     Compute group mean  $\mu_i \leftarrow \frac{1}{G} \sum_{k=1}^G r_{i,k}$ 
10:    for  $j = 1$  to  $G$  do
11:       $A_{i,j} \leftarrow r_{i,j} - \mu_i$ 
12:      ▷ Accumulate gradients over generation steps  $t$ 
13:       $\Delta\theta \leftarrow \Delta\theta + A_{i,j} \sum_{t=1}^{T_{i,j}} \nabla_\theta \log \pi_\theta(a_t | s_{<t})$ 
14:    end for
15:  end for
16:  Update parameters:  $\theta \leftarrow \theta + \alpha \cdot \frac{1}{B \cdot G} \Delta\theta$ 
17: until convergence

```

becomes redundant. We therefore maximize the objective $\mathcal{J}(\theta)$ by performing gradient ascent using the following estimator, which aggregates the gradient contributions across all generation steps t :

$$\nabla_\theta \mathcal{J}(\theta) \approx \frac{1}{BG} \sum_{i=1}^B \sum_{j=1}^G A_{i,j} \sum_{t=1}^{T_{i,j}} \nabla_\theta \log \pi_\theta(a_t | s_{<t}) \quad (2)$$

where a_t is the action selected at step t given the partial

graph $s_{<t}$.

The complete training procedure is summarized in Algorithm 1. By comparing molecules only against peers generated from the same starting molecular structure, GRX-Form learns effectively from both easy and hard starting structures simultaneously, stabilizing training across the heterogeneous chemical landscape.

4. Experiments

We evaluate the efficacy of GRXForm across three distinct tasks chosen to assess the framework’s capabilities in complementary settings: (1) broad structural generalization via goal-directed optimization of out-of-distribution molecular scaffolds; (2) few-shot rule transfer via a case study on pro-drug design; and (3) sample-efficient instance optimization via the PMO benchmark.

4.1. Task 1: Kinase Scaffold Decoration

Objective. Our primary evaluation focuses on the agent’s ability to elaborate unseen molecular scaffolds into valid biological inhibitors. We utilize the ZINC-250k dataset (Sterling & Irwin, 2015) as a source of scaffolds. To ensure the model generalizes to topologically distinct core structures rather than merely memorizing local patterns, we implement a cluster-based scaffold split (see Appendix C). First, we perform a Murcko Scaffold decomposition (Bemis & Murcko, 1996) using RDKit (Landrum, 2006). We then cluster these scaffolds using the Butina algorithm (Butina, 1999) based on Morgan fingerprints (Rogers & Hahn, 2010) with a strict Tanimoto similarity (Willett et al., 1998) cutoff of 0.4 for belonging to the same cluster. Entire clusters are then randomly assigned to the training, validation, or test sets, reserving 500 scaffolds for testing. We repeated this splitting procedure three times independently with different random seeds, generating three distinct train/validation/test sets. This procedure guarantees that test scaffolds are structurally distinct from training examples, occupying separate regions of the chemical embedding space (see Figure 5). The validation set was utilized to monitor the optimization score of the amortized models after each epoch, serving as the criterion for early stopping.

We define a Kinase Multi-Parameter Optimization (MPO) objective, following the protocol established by Jin et al. (2020). The reward $R(M)$ aggregates four components: biological activity against GSK3 β and JNK3 kinases (predicted via Random Forest models sourced from the Therapeutics Data Commons (TDC) library (Huang et al., 2021)), QED (drug-likeness), and Synthetic Accessibility (SA). We normalize SA to $[0, 1]$ via $SA' = (10 - SA)/9$. The training

reward is the mean of these components:

$$R(M) = \frac{1}{4} (P_{GSK3\beta} + P_{JNK3} + P_{QED} + P_{SA'}) \quad (3)$$

This smooth gradient facilitates stable learning. For evaluation, however, we adopt the strict binary success criterion from the same protocol (Jin et al., 2020): a molecule is deemed successful only if it simultaneously satisfies $P_{GSK3\beta} \geq 0.5$, $P_{JNK3} \geq 0.5$, $P_{QED} \geq 0.6$, and $SA \leq 4.0$.

Baselines and Ablations. We compare GRXForm against competitive models from both amortized and instance optimization paradigms that natively support structural elaboration (e.g., scaffold decoration). We exclude pure *de-novo* optimizers that require significant architectural redesign to handle substructure constraints.

- **Amortized Baselines:** We evaluate the original GraphXForm (trained via TASAR), LibINVENT, and DrugEx v3. We established a target budget of $\approx 50,000$ oracle calls to define a resource-constrained setting. While our proposed method (GRXForm) converges strictly within this limit, baselines utilizing different training paradigms (e.g., TASAR, DrugEx) required significantly more evaluations to reach stable performance (see Appendix E for a detailed breakdown of oracle consumption). During evaluation, all amortized models generate exactly one completion per test scaffold.

- **Instance Optimization Baselines:** We evaluate MolGA and GenMol. As these methods optimize from scratch for every input, they are allocated a maximum of 10,000 oracle calls *per test scaffold* (stopping early if convergence is reached); this represents a ceiling of 20% of our *total* training budget to optimize just a *single* test case. For the final evaluation metric, we select the single best completion found during the optimization trajectory for each test scaffold (see Appendix F for details). We note that for constrained generation, GenMol is primarily designed for single-iteration completion of an input structure by matching its pre-training distribution; attempting multi-iteration goal-directed optimization effectively demands a “chemist-in-the-loop” to manually select attachment sites, a limitation our approach avoids.

- **Ablations:** To validate our architectural choices, we evaluate: (1) **GRXForm-REINFORCE**, which replaces our Group Relative Policy Optimization (GRPO) with standard REINFORCE with a global baseline to test the necessity of group-specific normalization; and (2) **GRXForm-DeNovo**, an unconditional variant trained to construct molecules from scratch,

testing whether explicit conditional training is required for effective scaffold elaboration.

Implementation details are elaborated on in Appendix F.

Metrics. We report the objective score, i.e., the output of the reward function specified in Equation 3, and the success rate, defined as the percentage of test scaffolds yielding at least one valid molecule satisfying all hard thresholds.

Table 1. Performance comparison with baselines. Values represent the mean \pm standard deviation across three independent test folds. For each fold, the reported score is the average of the top completion found for each of the 500 test scaffolds.

METHOD	OBJ. SCORE (MEAN \pm STD)	SUCCESS RATE (MEAN \pm STD)
<i>Amortized Policies</i>		
GRAPHXFORM	0.409 \pm 0.003	0.000 \pm 0.000
LIBINVENT	0.371 \pm 0.004	0.000 \pm 0.000
DRUGEX V3	0.358 \pm 0.003	0.000 \pm 0.000
GRXFORM	0.618 \pm 0.004	0.178 \pm 0.093
<i>Instance Optimizers</i>		
MOL GA	0.438 \pm 0.013	0.000 \pm 0.000
GENMOL	0.441 \pm 0.012	0.000 \pm 0.000

Results and Analysis. The performance comparison on the held-out test set is presented in Table 1. GRXForm achieves a success rate of 17.8%, while all baselines failed to produce a single molecule satisfying the strict multiparameter success criteria (0% success rate). The failure of the amortized baselines (GraphXForm, LibINVENT, DrugEx v3) highlights the difficulty of *generalized* scaffold decoration. LibINVENT’s architecture, designed for optimizing single series, collapsed when tasked with diverse scaffolds. Similarly, DrugEx v3, despite its transformer backbone, failed to generalize the optimization logic to the unseen, topologically distinct test clusters.

Most notably, GRXForm outperformed the instance optimizers (Mol GA, GenMol) despite using orders of magnitude less compute per test instance. We attribute the failure of these baselines to the strict intersectional nature of the constraints combined with their specific search mechanics. For Mol GA, the standard genetic operators (mutation and crossover) frequently disrupt the core scaffold topology; enforcing preservation as a hard constraint (see Appendix F) leads to a high rejection rate of offspring, effectively stalling the evolutionary search before it can converge on the multi-objective targets. Regarding GenMol, we hypothesize that the performance gap stems from the mechanistic conflict between its optimization strategy and the strict topological constraints. GenMol relies on *Fragment Remasking* to optimize properties, a process the authors characterize as equivalent to Gibbs sampling. In its native setting, this allows

the model to iteratively rewrite any portion of the molecule. However, under strict scaffold constraints, the remasking process is artificially restricted solely to the side chains. This severely limits the degrees of freedom available to the denoising trajectory, effectively reducing the optimization process to a local random walk that struggles to locate the sparse solution manifold where all five constraints intersect. In contrast, GRXForm learns a conditional policy that explicitly models the distribution of valid, scaffold-preserving modifications. Beyond raw performance, we analyze the computational efficiency in Appendix E, demonstrating that GRXForm becomes more efficient than state-of-the-art instance optimizers after processing just 5 to 250 unique scaffolds, yielding significant net savings in high-throughput campaigns.

Table 2. Ablation study comparing purely *de-novo*, REINFORCE, and GRPO methods for GRXForm.

METHOD	OBJ. SCORE (MEAN \pm STD)	SUCCESS RATE (MEAN \pm STD)
GRXFORM-DENOVO	0.397 \pm 0.005	0.001 \pm 0.001
GRXFORM-REINFORCE	0.475 \pm 0.120	0.091 \pm 0.157
GRXFORM-GRPO	0.618 \pm 0.004	0.178 \pm 0.093

Ablation Study. Table 2 validates our architectural choices. The unconditional GRXForm-DeNovo baseline achieved a near-zero success rate (0.1%), confirming that explicit structural conditioning is necessary for this task. Furthermore, the GRXForm-REINFORCE baseline (global mean) achieved only 9.1% success with high variance ($std \pm 15.7\%$), significantly underperforming GRXForm-GRPO (17.8%). This confirms our hypothesis: normalizing rewards against a global baseline is ineffective when scaffold difficulty varies wildly. GRPO’s instance-specific normalization is important for stabilizing learning across

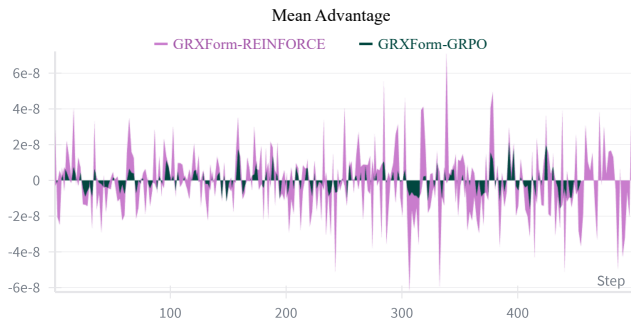


Figure 4. Advantage Signal Stability. Comparison of mean advantage during training. The global baseline (REINFORCE, pink) exhibits high-magnitude variance due to heterogeneous scaffold difficulty, destabilizing the gradient. In contrast, GRPO (green) mitigates this via instance-specific normalization, yielding a stable learning signal.

heterogeneous chemical space. Figure 4 provides empirical evidence of this instability, contrasting the volatile advantage signal of the global baseline against the stable, normalized signal of GRPO.

4.2. Task 2: Prodrug Transfer

We introduce a few-shot case study to evaluate whether the model can generalize a specific modification rule: *lipidization*. The objective is to transform a parent drug into a blood-brain barrier (BBB) permeable prodrug (an inactive precursor) by masking polar groups (hydroxyls, carboxyls) with lipophilic moieties. This must maximize ΔLogP while maintaining $\text{QED} > 0.5$ and the core pharmacophore. Unlike Task 1, this requires identifying specific functional handles for targeted modification.

Formally, using RDKit (Landrum, 2006), we define the reward $R(G, S_0)$ for a prodrug G from parent S_0 as:

$$R = \Delta\text{LogP} + \Delta\text{HBD} + \mathbb{I}_{\text{cleave}} + 2 \cdot \text{QED}(G) - 5 \cdot \mathbb{I}_{\text{MW} > 600} \quad (4)$$

Here, ΔLogP and ΔHBD reward lipophilicity and donor masking. The binary indicators $\mathbb{I}_{(\cdot)}$ return 1 if the condition is met: $\mathbb{I}_{\text{cleave}}$ detects hydrolyzable linkages via SMARTS, while $\mathbb{I}_{\text{MW} > 600}$ penalizes weights > 600 Da to prevent trivial elongation.

Experimental Setup. We evaluate the same model variants introduced in Task 1: GRXForm-GRPO and the baseline GRXForm-REINFORCE. Starting from a common checkpoint pre-trained on ChEMBL version 35, both models were fine-tuned in a few-shot protocol on only 4 exemplar drugs: Morphine, GABA, Nipecotic Acid, and Aspirin. We evaluate on 5 held-out drugs that possess similar functional groups but *unseen structures* to test transferability. For each test drug, we sample one completion (molecule) from the policy. We treat this task primarily as a case study to assess the practicality and ablation of our contributions in a realistic drug discovery scenario. Consequently, we exclude external baselines, as they typically require the manual specification of attachment points for structural modification, whereas this task specifically evaluates the agent’s ability to autonomously identify valid modification sites.

Results. Table 3 presents the objective scores for GRXForm-REINFORCE versus GRXForm-GRPO. The baseline exhibited significant performance degradation on complex inputs. Notably, on Naltrexone (a complex tetracyclic opiate), the baseline failed to find a high-scoring solution (Score: 1.71), whereas GRXForm successfully optimized the structure (Score: 7.54). Overall, GRXForm achieved a higher score on all 5 test cases and a higher mean performance. This suggests that normalizing rewards relative to the specific starting structure allows the policy to learn a more robust optimization strategy that generalizes effectively to unseen

and structurally diverse drugs.

Table 3. Performance comparison on the held-out test set for the Prodrug Transfer task. Scores indicate the objective value (higher is better).

TEST DRUG (UNSEEN)	GRXFORM (REINFORCE)	GRXFORM (GRPO)
NALTREXONE	1.707	7.542
LEVODOPA	10.165	11.685
BACLOFEN	12.614	12.665
SEROTONIN	10.682	11.112
NAPROXEN	8.092	10.462
MEAN	8.652	10.693

4.3. Task 3: PMO Benchmark

To assess performance against a wider array of objectives, we evaluate GRXForm on the PMO benchmark (Table 4). This suite defines a set of standard *de-novo* molecular design tasks with a constrained budget of 10,000 oracle calls per task. To strictly adhere to this protocol, we run GRXForm as an instance optimizer for *de-novo* design using online reinforcement learning. We fine-tune the policy using standard REINFORCE with a global baseline, utilizing the allotted 10,000 oracle calls as the online training budget (see Appendix D for protocol details). The benchmark evaluates sample efficiency using the Area Under the Curve (AUC) of the top-10 property scores. We compare GRXForm against state-of-the-art baselines reported in Lee et al. (2025) on 22 of the 23 standard PMO tasks. We exclude *Valsartan SMARTS* following Lo et al. (2025) (see Appendix D).

Results. Based on the results in Table 4, GRXForm demonstrates strong sample efficiency, achieving a cumulative AUC top-10 score of 16.433. This performance secures the second-highest rank overall, marginally outperforming the synthesis-aware baseline SynGBO (16.426) and the retrieval-augmented method f-RAG (16.301). While the discrete diffusion model GenMol achieves the highest aggregate score, GRXForm remains highly competitive, delivering strong results among amortized policies and outperforming several established instance optimization baselines such as Genetic GFN (16.078) and Mol GA (15.686).

We emphasize that this benchmark isolates raw *de-novo* optimization capability, intentionally disregarding the significant inference-speed advantages offered by amortization. These results therefore serve to validate that GRXForm secures the generalization benefits of a transferable policy without sacrificing the peak optimization power typically associated with computationally intensive, single-instance search methods.

5. Conclusion

GRXForm demonstrates that the computational burden of molecular optimization can be effectively shifted from inference-time search to training-time learning. Our key conceptual insight is that when training an RL policy for molecular generation, we must account for the high variance in the difficulty of successful molecular generation across different initial structures. We address this by adapting GRPO; our ablation studies demonstrate that this mechanism is essential for the method’s success. By enforcing chemical validity through the model architecture and stabilizing the learning process with group-relative baselines, we achieve a policy capable of fast, generalized optimization. This approach offers a scalable alternative to iterative search methods, enabling high-throughput design without the prohibitive cost of repeated oracle evaluations. Looking forward, we plan to evaluate the framework on tasks requiring atom and bond removal (e.g., scaffold morphing, lead optimization) and linking disjoint fragments. Finally, we find combining the benefits of instance optimization and amortization particularly interesting as an avenue for future work.

Impact Statement

This work advances the field of automated drug discovery by introducing a computationally efficient, amortized optimization framework. By significantly reducing the inference-time cost of molecular design compared to iterative search methods, our approach lowers the energy footprint of high-throughput screening. However, given the potential for dual-use in generative chemistry, we emphasize the necessity of human oversight and ethical due diligence to prevent the design of harmful compounds.

Acknowledgements

Muhammad bin Javaid was supported by the Werner Siemens Foundation within the WSS project of the century “catalaix”.

Ashima Khanna, Jonathan Pirnay, and Dominik G. Grimm were supported by the Deutsche Forschungsgemeinschaft (DFG, German Research Foundation) grant 466387255 within the Priority Programme “SPP 2331: Machine Learning in Chemical Engineering”.

Berke Kişin and Martin Grohe were supported by the Deutsche Forschungsgemeinschaft (DFG, German Research Foundation) grant GR 1492/20-2 within the Priority Programme “SPP 2331: Machine Learning in Chemical Engineering” and the Werner Siemens Foundation within the WSS project of the century “catalaix”.

Alexander Mitsos was supported by the Deutsche

Forschungsgemeinschaft (DFG, German Research Foundation) grant 466417970 within the Priority Programme “SPP 2331: Machine Learning in Chemical Engineering” and the Werner Siemens Foundation within the WSS project of the century “catalaix”.

References

Avdeyev, P., Shi, C., Tan, Y., Dudnyk, K., and Zhou, J. Dirichlet Diffusion Score Model for biological sequence generation. In *International Conference on Machine Learning*, 2023. URL <https://arxiv.org/abs/2305.10699>.

Bachlechner, T., Majumder, B. P., Mao, H., Cottrell, G., and McAuley, J. Rezero is all you need: Fast convergence at large depth. In *Uncertainty in Artificial Intelligence*, pp. 1352–1361. PMLR, 2021.

Bemis, G. W. and Murcko, M. A. The properties of known drugs. 1. molecular frameworks. *Journal of medicinal chemistry*, 39(15):2887–2893, 1996.

Bengio, E., Jain, M., Korablyov, M., Precup, D., and Bengio, Y. Flow network based generative models for non-iterative diverse candidate generation. In Beygelzimer, A., Dauphin, Y., Liang, P., and Vaughan, J. W. (eds.), *Advances in Neural Information Processing Systems*, 2021. URL <https://openreview.net/forum?id=Arn2E4IRjEB>.

Bickerton, G. R., Paolini, G. V., Besnard, J., Muresan, S., and Hopkins, A. L. Quantifying the chemical beauty of drugs. *Nature chemistry*, 4(2):90–98, 2012.

Butina, D. Unsupervised data base clustering based on daylight’s fingerprint and tanimoto similarity: A fast and automated way to cluster small and large data sets. *Journal of Chemical Information and Computer Sciences*, 39(4):747–750, 1999.

Chen, Z., Min, M. R., Parthasarathy, S., and Ning, X. A deep generative model for molecule optimization via one fragment modification. *Nature Machine Intelligence*, 3(12):1040–1049, Dec 2021. ISSN 2522-5839. doi: 10.1038/s42256-021-00410-2. URL <https://doi.org/10.1038/s42256-021-00410-2>.

Chu, T., Zhai, Y., Yang, J., Tong, S., Xie, S., Schuurmans, D., Le, Q. V., Levine, S., and Ma, Y. SFT memorizes, RL generalizes: A comparative study of foundation model post-training. In *Forty-second International Conference on Machine Learning*, 2025. URL <https://openreview.net/forum?id=dYur3yabMj>.

Davies, M., Nowotka, M., Papadatos, G., Dedman, N., Gaulton, A., Atkinson, F., Bellis, L., and Overington, M. J. A deep generative model for molecule optimization via one fragment modification. *Nature Machine Intelligence*, 3(12):1040–1049, Dec 2021. ISSN 2522-5839. doi: 10.1038/s42256-021-00410-2. URL <https://doi.org/10.1038/s42256-021-00410-2>.

J. P. ChembL web services: streamlining access to drug discovery data and utilities. *Nucleic Acids Research*, 43 (W1):W612–W620, 04 2015. ISSN 0305-1048. doi: 10.1093/nar/gkv352. URL <https://doi.org/10.1093/nar/gkv352>.

Fu, T., Xiao, C., Li, X., Glass, L. M., and Sun, J. Mimosa: Multi-constraint molecule sampling for molecule optimization. In *Proceedings of the AAAI Conference on Artificial Intelligence*, volume 35, pp. 125–133, 2021.

Gao, W., Fu, T., Sun, J., and Coley, C. W. Sample efficiency matters: A benchmark for practical molecular optimization. In *Thirty-sixth Conference on Neural Information Processing Systems Datasets and Benchmarks Track*, 2022. URL <https://openreview.net/forum?id=yCZRdI0Y7G>.

Ghugare, R., Geist, M., Berseth, G., and Eysenbach, B. Closing the gap between TD learning and supervised learning - a generalisation point of view. In *The Twelfth International Conference on Learning Representations*, 2024. URL <https://openreview.net/forum?id=qg5JENs0N4>.

Haarnoja, T., Zhou, A., Abbeel, P., and Levine, S. Soft actor-critic: Off-policy maximum entropy deep reinforcement learning with a stochastic actor. In *International conference on machine learning*, pp. 1861–1870. Pmlr, 2018.

Hetzel, L., Sommer, J., Rieck, B., Theis, F., and Gündemann, S. Magnet: Motif-agnostic generation of molecules from shapes. *arXiv preprint arXiv:2305.19303*, 2023.

Huang, K., Fu, T., Gao, W., Zhao, Y., Roohani, Y., Leskovec, J., Coley, C. W., Xiao, C., Sun, J., and Zitnik, M. Therapeutics data commons: Machine learning datasets and tasks for drug discovery and development. *Proceedings of Neural Information Processing Systems, NeurIPS Datasets and Benchmarks*, 2021.

Hughes, J. P., Rees, S., Kalindjian, S. B., and Philpott, K. L. Principles of early drug discovery. *British journal of pharmacology*, 162(6):1239–1249, 2011.

Jensen, J. H. A graph-based genetic algorithm and generative model/monte carlo tree search for the exploration of chemical space. *Chemical science*, 10(12):3567–3572, 2019.

Jin, W., Barzilay, R., and Jaakkola, T. Junction tree variational autoencoder for molecular graph generation. In *International conference on machine learning*, pp. 2323–2332. PMLR, 2018.

Jin, W., Barzilay, R., and Jaakkola, T. Multi-objective molecule generation using interpretable substructures. In *International conference on machine learning*, pp. 4849–4859. PMLR, 2020.

Kim, H., Kim, M., Choi, S., and Park, J. Genetic-guided GFlownets for sample efficient molecular optimization. In *The Thirty-eighth Annual Conference on Neural Information Processing Systems*, 2024. URL <https://openreview.net/forum?id=B4q98aAZwt>.

Kong, X., Huang, W., Tan, Z., and Liu, Y. Molecule generation by principal subgraph mining and assembling. *Advances in Neural Information Processing Systems*, 35: 2550–2563, 2022.

Kool, W., Van Hoof, H., and Welling, M. Stochastic beams and where to find them: The gumbel-top-k trick for sampling sequences without replacement. In *International conference on machine learning*, pp. 3499–3508. PMLR, 2019.

Landrum, G. Rdkit: Open-source cheminformatics, 2006. URL <http://www.rdkit.org>. accessed 2026-01-11.

Lee, S., Kreis, K., Veccham, S. P., Liu, M., Reidenbach, D., Paliwal, S., Vahdat, A., and Nie, W. Molecule generation with fragment retrieval augmentation. *Advances in Neural Information Processing Systems*, 2024.

Lee, S., Kreis, K., Veccham, S. P., Liu, M., Reidenbach, D., Peng, Y., Paliwal, S. G., Nie, W., and Vahdat, A. Genmol: A drug discovery generalist with discrete diffusion. In *Forty-second International Conference on Machine Learning*, 2025. URL <https://openreview.net/forum?id=KM7pXWG1xj>.

Liu, X., Ye, K., van Vlijmen, H. W. T., IJzerman, A. P., and van Westen, G. J. P. Drugex v3: scaffold-constrained drug design with graph transformer-based reinforcement learning. *Journal of Cheminformatics*, 15(1): 24, Feb 2023. ISSN 1758-2946. doi: 10.1186/s13321-023-00694-z. URL <https://doi.org/10.1186/s13321-023-00694-z>.

Liu, Z., Chen, C., Li, W., Qi, P., Pang, T., Du, C., Lee, W. S., and Lin, M. Understanding r1-zero-like training: A critical perspective. In *Conference on Language Modeling (COLM)*, 2025.

Lo, A., Coley, C. W., and Matusik, W. A genetic algorithm for navigating synthesizable molecular spaces. *arXiv preprint arXiv:2509.20719*, 2025.

Loeffler, H. H., He, J., Tibo, A., Janet, J. P., Voronov, A., Mervin, L. H., and Engkvist, O. Reinvent 4: Modern ai-driven generative molecule design. *Journal of*

Cheminformatics, 16(1):20, Feb 2024. ISSN 1758-2946. doi: 10.1186/s13321-024-00812-5. URL <https://doi.org/10.1186/s13321-024-00812-5>.

Luo, Y., Yan, K., and Ji, S. Graphdf: A discrete flow model for molecular graph generation. In *International conference on machine learning*, pp. 7192–7203. PMLR, 2021.

Maziarz, K., Jackson-Flux, H. R., Cameron, P., Sirockin, F., Schneider, N., Stiefl, N., Segler, M., and Brockschmidt, M. Learning to extend molecular scaffolds with structural motifs. In *International Conference on Learning Representations*, 2022. URL <https://openreview.net/forum?id=ZTsoE8G3GG>.

Mercado, R., Rastemo, T., Lindelöf, E., Klambauer, G., Engkvist, O., Chen, H., and Bjerrum, E. J. Graph Networks for Molecular Design. *Machine Learning: Science and Technology*, 2020. doi: 10.1088/2632-2153/abcf91.

Noutahi, E., Gabellini, C., Craig, M., Lim, J. S., and Tossou, P. Gotta be safe: a new framework for molecular design. *Digital Discovery*, 3(4):796–804, 2024.

Olivecrona, M., Blaschke, T., Engkvist, O., and Chen, H. Molecular de-novo design through deep reinforcement learning. *Journal of Cheminformatics*, 9(1):48, Sep 2017. ISSN 1758-2946. doi: 10.1186/s13321-017-0235-x. URL <https://doi.org/10.1186/s13321-017-0235-x>.

Pirnay, J. and Grimm, D. G. Self-improvement for neural combinatorial optimization: Sample without replacement, but improvement. *Transactions on Machine Learning Research*, 2024a. ISSN 2835-8856. URL <https://openreview.net/forum?id=agT8ojoH0X>. Featured Certification.

Pirnay, J. and Grimm, D. G. Take a step and reconsider: Sequence decoding for self-improved neural combinatorial optimization. In Endriss, U., Melo, F., Bach, K., Bugarin-Diz, A., Alonso-Moral, J., Barro, S., and Heintz, F. (eds.), *ECAI 2024 - 27th European Conference on Artificial Intelligence, Including 13th Conference on Prestigious Applications of Intelligent Systems, PAIS 2024, Proceedings*, Frontiers in Artificial Intelligence and Applications, pp. 1927–1934. IOS Press BV, October 2024b. doi: 10.3233/FAIA240707. Publisher Copyright: © 2024 The Authors.; 27th European Conference on Artificial Intelligence, ECAI 2024 ; Conference date: 19-10-2024 Through 24-10-2024.

Pirnay, J., Rittig, J. G., Wolf, A. B., Grohe, M., Burger, J., Mitsos, A., and Grimm, D. G. Graphxform: graph transformer for computer-aided molecular design. *Digital Discovery*, 4:1052–1065, 2025. doi: 10.1039/D4DD00339J. URL <http://dx.doi.org/10.1039/D4DD00339J>.

Rennie, S. J., Marcheret, E., Mroueh, Y., Ross, J., and Goel, V. Self-critical sequence training for image captioning. In *Proceedings of the IEEE conference on computer vision and pattern recognition*, pp. 7008–7024, 2017.

Rogers, D. and Hahn, M. Extended-connectivity fingerprints. *Journal of chemical information and modeling*, 50(5):742–754, 2010.

Schulman, J., Wolski, F., Dhariwal, P., Radford, A., and Klimov, O. Proximal policy optimization algorithms. *arXiv preprint arXiv:1707.06347*, 2017.

Shao, Z., Wang, P., Zhu, Q., Xu, R., Song, J., Bi, X., Zhang, H., Zhang, M., Li, Y. K., Wu, Y., and et al. DeepSeekMath: Pushing the Limits of Mathematical Reasoning in Open Language Models. *arXiv e-prints*, art. arXiv:2402.03300, February 2024. doi: 10.48550/arXiv.2402.03300.

Shen, T., Seo, S., Lee, G., Pandey, M., Smith, J. R., Cherkasov, A., Kim, W. Y., and Ester, M. TacoGFN: Target-conditioned GFlownet for structure-based drug design. *Transactions on Machine Learning Research*, 2024. ISSN 2835-8856. URL <https://openreview.net/forum?id=N8cPv95zOU>.

Shi*, C., Xu*, M., Zhu, Z., Zhang, W., Zhang, M., and Tang, J. Graphaf: a flow-based autoregressive model for molecular graph generation. In *International Conference on Learning Representations*, 2020. URL <https://openreview.net/forum?id=S1esMkHYPr>.

Song, M. Good actions succeed, bad actions generalize: A case study on why RL generalizes better. In *Second Workshop on Out-of-Distribution Generalization in Robotics at RSS 2025*, 2025. URL <https://openreview.net/forum?id=TQLulojaZp>.

Sterling, T. and Irwin, J. J. Zinc 15 – ligand discovery for everyone. *Journal of Chemical Information and Modeling*, 55(11):2324–2337, Nov 2015. ISSN 1549-9596. doi: 10.1021/acs.jcim.5b00559. URL <https://doi.org/10.1021/acs.jcim.5b00559>.

Tripp, A. and Hernández-Lobato, J. M. Genetic algorithms are strong baselines for molecule generation. *arXiv preprint arXiv:2310.09267*, 2023.

Vignac, C., Krawczuk, I., Sirauidin, A., Wang, B., Cevher, V., and Frossard, P. Digress: Discrete denoising diffusion for graph generation. In *The Eleventh International Conference on Learning Representations*, 2023. URL <https://openreview.net/forum?id=UaAD-Nu86WX>.

Wang, Z., Nie, W., Qiao, Z., Xiao, C., Baraniuk, R., and Anandkumar, A. Retrieval-based controllable molecule generation. *arXiv preprint arXiv:2208.11126*, 2022.

Wildman, S. A. and Crippen, G. M. Prediction of physicochemical parameters by atomic contributions. *Journal of chemical information and computer sciences*, 39(5):868–873, 1999.

Willett, P., Barnard, J. M., and Downs, G. M. Chemical similarity searching. *Journal of chemical information and computer sciences*, 38(6):983–996, 1998.

Winter, R., Montanari, F., Steffen, A., Briem, H., Noé, F., and Clevert, D.-A. Efficient multi-objective molecular optimization in a continuous latent space. *Chem. Sci.*, 10:8016–8024, 2019. doi: 10.1039/C9SC01928F. URL <http://dx.doi.org/10.1039/C9SC01928F>.

Xie, Y., Shi, C., Zhou, H., Yang, Y., Zhang, W., Yu, Y., and Li, L. {MARS}: Markov molecular sampling for multi-objective drug discovery. In *International Conference on Learning Representations*, 2021. URL <https://openreview.net/forum?id=kHSu4ebxFXY>.

Yang, S., Hwang, D., Lee, S., Ryu, S., and Hwang, S. J. Hit and lead discovery with explorative rl and fragment-based molecule generation. *Advances in Neural Information Processing Systems*, 34:7924–7936, 2021.

Yang, Y., Zheng, S., Su, S., Zhao, C., Xu, J., and Chen, H. Syntalink: automatic fragment linking with deep conditional transformer neural networks. *Chemical science*, 11(31):8312–8322, 2020.

You, J., Liu, B., Ying, Z., Pande, V., and Leskovec, J. Graph convolutional policy network for goal-directed molecular graph generation. In Bengio, S., Wallach, H., Larochelle, H., Grauman, K., Cesa-Bianchi, N., and Garnett, R. (eds.), *Advances in Neural Information Processing Systems*, volume 31. Curran Associates, Inc., 2018. URL https://proceedings.neurips.cc/paper_files/paper/2018/file/d60678e8f2ba9c540798ebbde31177e8-Paper.pdf.

Zhou, Z., Kearnes, S., Li, L., Zare, R. N., and Riley, P. Optimization of molecules via deep reinforcement learning. *Scientific Reports*, 9(1):10752, Jul 2019. ISSN 2045-2322. doi: 10.1038/s41598-019-47148-x. URL <https://doi.org/10.1038/s41598-019-47148-x>.

A. Taxonomy of Generative Optimization

We structure our analysis of the generative molecular design landscape through the lens of two distinct optimization paradigms: instance optimization, which treats every design task as a unique search problem to be solved from scratch, and amortized optimization, which distills optimization logic into a learned policy which can be re-used.

A.1. Instance Optimization

Methods in this category treat molecular design as a combinatorial optimization problem. They rely on an external oracle (scoring function) to guide a traversal of chemical space during the inference phase. While often effective at finding high-scoring molecules, they suffer from high computational cost and a lack of transferable knowledge.

Genetic Algorithms and MCMC. Evolutionary strategies remain formidable baselines in drug discovery. Methods such as Graph-GA and Mol GA (Jensen, 2019; Tripp & Hernández-Lobato, 2023) evolve a population of molecular graphs through crossover and mutation operations. These classical frameworks often outperform deep learning methods, with Mol GA achieving good performance in sample efficiency tasks such as the PMO benchmark. However, they are computationally expensive, typically requiring thousands of oracle evaluations per target task to effectively navigate the chemical space, making them impractical for high-throughput scenarios or expensive biological oracles. Similarly, Markov Chain Monte Carlo (MCMC) approaches like MARS (Xie et al., 2021) and MIMOSA (Fu et al., 2021) navigate chemical space by iteratively editing molecules (adding/deleting bonds or atoms) via a proposal network. As these methods optimize a single instance via repeated sampling steps, they are operationally distinct from amortized policies.

Latent Space Search (VAEs) Deep generative models based on Variational Autoencoders (VAEs), such as JT-VAE (Jin et al., 2018), MoLeR (Maziarz et al., 2022), and MAGNet (Hetzell et al., 2023) map discrete molecular graphs to a continuous latent space. To perform optimization, these frameworks rely on inference-time search algorithms such as Bayesian Optimization or Molecular Swarm Optimization (Winter et al., 2019) to traverse the latent manifold and decode new candidates. Consequently, the “generative” step is a decoding operation for an underlying search process. Similarly, deep editing models like Modof (Chen et al., 2021) are trained to predict single-step structural modifications (e.g., disconnection and replacement). To achieve significant structural elaboration, such models must be applied iteratively in a loop, effectively reverting to a search-based instance optimization paradigm rather than single-pass generation.

Discrete Diffusion and Iterative Refinement. Recently, discrete diffusion models have been applied to molecular graphs (Vignac et al., 2023) and sequences (Avdeyev et al., 2023). While such frameworks technically support molecule completion (inpainting) by fixing scaffold nodes during the reverse process, we exclude them as direct baselines because they function primarily as distribution learners rather than optimizers. Conditional sampling $p_\theta(x|\text{scaffold})$ is strictly bound by the quality of the training data; in the absence of dense, high-reward examples in the training set (the exploration gap), standard diffusion lacks the extrapolation capability to discover novel, high-performing solutions.

To bridge this gap, state-of-the-art approaches like GenMol (Lee et al., 2025) must reintroduce inference-time search. GenMol serves as a generalist model using Sequential Attachment-based Fragment Embedding (SAFE) (Noutahi et al., 2024) with a non-autoregressive, bidirectional parallel decoding scheme. However, to perform goal-directed tasks like lead optimization, it relies explicitly on an iterative “fragment remasking” loop. As the authors note, this process functions as a mutation operation where specific fragments are masked and regenerated iteratively based on oracle feedback. This effectively constitutes a guided random walk (Gibbs sampling) in the neighborhood of a seed molecule. Consequently, GenMol functions as an instance optimizer: it does not learn a direct, amortized mapping from a starting structure to an optimized molecule, but rather relies on a computationally expensive denoising kernel to actively search chemical space at test time.

A.2. Amortized Optimization (Learned Policies)

Prior-Regularized RL. To ensure chemical validity, frameworks like REINVENT (Olivecrona et al., 2017) and GraphINVENT (Mercado et al., 2020) rely on anchored strategies (e.g., Direct Augmented Likelihood), which explicitly regularize the reward with a fixed pre-trained prior. This prior serves to constrain the agent to the training distribution. While this helps ensures chemical validity, it introduces a trade-off: maximizing the reward often requires drifting far from the prior, which the regularization term actively resists. Consequently, achieving high scores on specific targets requires an iterative learning process to gradually shift the agent’s distribution.

Stepwise Graph Construction. Early deep reinforcement learning approaches formulated molecular design as a Markov Decision Process (MDP) operating at the atom level. GCPN (You et al., 2018) employs a Graph Convolutional Policy Network to construct molecules node-by-node and edge-by-edge, using Proximal Policy Optimization (PPO) (Schulman et al., 2017) to update the policy. By treating valency checks as intermediate environment rewards, it learns to generate valid structures. MolDQN (Zhou et al., 2019) approaches the same MDP formulation through using Double Q-Learning to greedily select atoms and bonds that maximize the expected future reward.

Flow-based Models. Normalizing flows model the molecular distribution $p(x)$ by learning an invertible mapping between molecular graphs and a latent base distribution. To perform goal-directed optimization, these frameworks typically employ a two-stage paradigm: pre-training on a large dataset to learn chemical validity, followed by RL fine-tuning. GraphAF (Shi* et al., 2020) formulates generation as an autoregressive flow; however, to apply continuous dynamics to discrete graphs, it relies on dequantization (adding real-valued noise), which introduces stochasticity that hinders the precise optimization of property constraints. To resolve this, GraphDF (Luo et al., 2021) replaces continuous transformations with discrete latent variables using invertible modulo shift transforms. By eliminating dequantization noise, GraphDF provides a more stable mapping for the RL agent, enabling more efficient navigation of the chemical property landscape.

Generative Flow Networks (GFlowNets). Generative Flow Networks (GFlowNets) (Bengio et al., 2021) are designed to learn a stochastic policy that samples candidates with probability proportional to their reward. While theoretically powerful for diverse mode coverage, prioritizing this diversity can trade off against the rapid peak-finding required in sparse, high-dimensional chemical spaces, as suggested by the relatively poor performance of GFlowNets on the PMO benchmark. To address this, hybrid methods such as Genetic GFN (Kim et al., 2024) augment training with evolutionary operators; however, this shifts the paradigm back toward instance optimization. By relying on a GA to populate the replay buffer with task-specific elite solutions, Genetic GFN focuses on solving the current instance rather than learning a generalizable policy for new constraints or scaffolds without restarting the online training loop. Crucially, we distinguish our approach from standard GFlowNets based on the structural requirements of the design task. The canonical GFlowNet formulation relies on a fixed root state s_0 (typically an empty graph). While architectures like TacoGFN (Shen et al., 2024) solve target-conditional generation (e.g., conditioning on a protein pocket), they still initiate flow from the empty graph. To enforce a structural hard-constraint (e.g., the output must contain the subgraph C) in this setting, the agent is forced to reconstruct the subgraph C from scratch. This introduces an exploration bottleneck, as the model must correctly navigate a long, specific trajectory simply to reproduce the input before optimization can begin. Alternatively, treating the scaffold itself as the starting root ($s_0 = C$) requires the framework to handle variable starting states; a non-trivial adaptation that effectively requires training a distinct flow for each unique scaffold (instance optimization) or fundamental architectural redesign. Consequently, we focus our comparison on paradigms that natively support the variable-starting point regime.

Fragment-Based Methods. To improve optimization efficiency and ensure local substructure validity, methods like FREED (Yang et al., 2021) and SAFE-GPT (Noutahi et al., 2024) elevate the action space from atoms to fragments. FREED sequentially attaches chemically valid fragments to a growing structure and uses Soft Actor-Critic (SAC) (Haarnoja et al., 2018) to update the model, while SAFE-GPT leverages a textual fragment representation (SAFE) to generate molecules token-by-token and uses PPO to update the model. Unlike the vocabulary-mining approaches (discussed below) which focus on extracting specific rationales, these methods focus on learning a flexible policy to assemble a fixed library of fragments.

Retrieval-Augmented Generation (RAG) and Vocabulary-Based Methods. A distinct subset of methods grounds the optimization process by recalling known high-value substructures. To circumvent the sparsity of high-reward molecules, RationaleRL (Jin et al., 2020) and PS-VAE (Kong et al., 2022) rely on vocabulary construction. RationaleRL employs offline MCTS to mine property-specific “rationales” (active subgraphs), while PS-VAE extracts “Principal Subgraphs,” defined as high-frequency motifs that minimize reconstruction error across the training set. By treating generation as the completion of these rigid building blocks, these methods amortize the search cost. However, they suffer from vocabulary rigidity: exploration is bounded by the combinatorial closure of the pre-extracted fragments. To address this rigidity, recent approaches introduce inference-time retrieval loops, shifting towards instance optimization. RetMol (Wang et al., 2022) employs a “soft” retrieval paradigm, fetching whole exemplar molecules to fuse into the generator’s latent space. It relies on an iterative refinement procedure: generating candidates, evaluating them with the oracle, and updating the retrieval database dynamically. Similarly, f-RAG (Lee et al., 2024) utilizes a dual-retrieval mechanism (fetching both “hard” structural anchors and “soft” latent guidance). By updating its fragment memory online during exploration, f-RAG effectively reintroduces a search component, using the learned policy to accelerate the discovery of high-scoring fragments that are then stored for subsequent retrieval.

Conditional Encoder-Decoder Models. Distinct from stepwise graph construction, these models treat scaffold decoration as a translation task: mapping a starting scaffold to a completed molecule. SyntaLinker (Yang et al., 2020) applies this paradigm to 1D sequences, utilizing a Transformer to “translate” fragment pairs into linked molecules. In the graph domain, DrugEx v3 (Liu et al., 2023) employs an encoder-decoder Graph Transformer trained via a multi-objective REINFORCE algorithm. It explicitly conditions on the scaffold input, learning a policy to generate complementary structures. To manage the high variance typical of policy gradient updates, DrugEx v3 relies on a Pareto-based ranking strategy and an explicit “exploration network” (a fixed, pre-trained copy of the policy) to force diverse sampling. However, unlike our approach which normalizes rewards relative to the specific scaffold instance (GRPO), DrugEx v3’s updates utilize a global reward formulation. Consequently, to prevent mode collapse on difficult scaffolds, it must rely on external exploration heuristics rather than an intrinsic variance-reduction mechanism.

Search-Based Imitation Learning. A hybrid approach involves training a policy to imitate the trajectory of a search algorithm. The original GraphXForm (Pirnay et al., 2025) employs a Self-Improvement Learning (SIL) loop, combining the Deep Cross-Entropy Method (CEM) with a sequence decoding algorithm “Take a Step and Reconsider” (TASAR) (Pirnay & Grimm, 2024b). In this paradigm, the model generates candidate sequences, evaluates them with the oracle, and selects the highest-scoring trajectories as pseudo-labels for supervised fine-tuning. While this stabilizes training without value approximation, it remains computationally expensive during the training phase. It is a known phenomenon that supervised (imitation) learning generalizes less effectively than reinforcement learning (Song, 2025; Ghugare et al., 2024; Chu et al., 2025).

Our Approach: GRXForm incorporates the structural inductive biases of Graph Transformers while utilizing atom-level stepwise graph construction, and amortizes the optimization cost effectively into a learned policy. Instead of relying on a restrictive prior or a hard-to-train value network, we employ GRPO. By using group-based statistics as a dynamic baseline, GRPO stabilizes the learning of constructive design rules across diverse starting points.

B. GRXForm Architecture

B.1. Action Space

We model molecular generation as a sequential Markov Decision Process. A state s_t represents the intermediate partial molecular graph at step t . This graph consists of a set of atoms V_t (with properties such as element type, charge, etc.) and bonds E_t .

The action space \mathcal{A} is decomposed hierarchically to account for the discrete nature of graph construction. To transition from state s_t to state s_{t+1} , the policy samples a composite action that is decomposed into three sequential sub-levels. This decomposition reduces the combinatorial complexity of the action space:

- 1. Action Level 0 (Operation Selection):** The agent first decides the nature of the modification. It produces a distribution over three categories of moves:
 - *Termination*: The STOP token, ending the generation process.
 - *Add Atom*: Selecting a new element type $T \in \Sigma$ (e.g., C, N, O, ...) from the vocabulary to add to the graph. For all our experiments, the vocabulary size is 23 (see Appendix B.2 for details).
 - *Modify Existing*: Selecting an existing atom $u \in V_t$ to serve as the source of a new bond.
- 2. Action Level 1 (Target Selection):** Conditional on the first selection, the agent selects a target atom $v \in V_t$. If a new atom type was selected in Level 0, this step determines the anchor point v on the existing graph to which the new atom connects. If an existing atom u was selected in Level 0, v represents the destination of a new bond starting from u .
- 3. Action Level 2 (Bond Specification):** Finally, the agent determines the bond order $b \in \{1, 2, 3, 4, 5, 6\}$ for the edge connecting the two atoms identified in the previous steps.

To ensure chemical validity, we employ a validity mask $\mathcal{M}(s_t)$. At each action level, probabilities of actions that would violate valence constraints (e.g., exceeding the maximum bond capacity of an atom) are masked to zero. This guarantees that every sampled trajectory remains within the subspace of chemically valid graphs.

B.2. Atom Vocabulary

The generative model uses a fixed vocabulary of 23 atomic tokens, representing specific combinations of element, formal charge, and chirality. The allowed tokens are:

- **Carbon:** C, C⁺, C⁻, C@, C@@
- **Nitrogen:** N, N⁺, N⁻
- **Oxygen:** O, O⁺, O⁻
- **Phosphorus:** P, P⁺, P⁻
- **Sulfur:** S, S⁺, S⁻, S@, S@@
- **Halogens:** F, Cl, Br, I

Note: @ and @@ denote tetrahedral chirality attributes.

B.3. Policy Architecture

We parameterize the policy π_θ using a decoder-only Graph Transformer that processes the molecule as an unordered set of atoms. To capture global context and aggregate sequence-level information, the graph is augmented with a virtual “super-node” v_{virtual} connected to all atoms via special edges.

Input Representation. The input to the model is the set of atoms in the current partial graph. To condition the policy on the sequential sub-actions (e.g., informing Level 1 which atom was picked in Level 0), we augment the standard atom features with dynamic state embeddings. The input embedding h_i for the i -th atom is the sum of:

- **Atom Type Embedding:** A learnable vector representing the element type.
- **Degree Embedding:** Encoding the current number of bonds connected to the atom.
- **Action State Embeddings:** Two binary embedding vectors $w_i^{(0)}$ and $w_i^{(1)}$ which indicate whether atom i was selected at Action Level 0 or Level 1, respectively. This allows the transformer to “focus” on the active atoms during the multi-step decision process.

Graph Transformer Layers. These embeddings are processed through L layers of Multi-Head Self-Attention (MHSA) with ReZero normalization (Bachlechner et al., 2021). We do not use positional encodings, preserving permutation equivariance. Structural topology is injected directly into the attention mechanism via bias terms. The attention score A_{ij} between atoms i and j is computed as:

$$A_{ij} = \text{softmax} \left(\frac{Q_i K_j^T}{\sqrt{d_k}} + \phi(e_{ij}) \right) \quad (5)$$

where $\phi(e_{ij})$ is a learnable scalar bias derived from the bond order e_{ij} connecting the atoms. This allows the model to attend to topological neighbors differently than distant atoms.

Action Heads. The final node representations are projected via separate Multi-Layer Perceptrons (MLPs) to produce logits for the three action levels. The Level 0 head projects the virtual node representation to predict STOP or new atom types, and projects individual atom representations to predict the selection of existing atoms. Levels 1 and 2 operate similarly, conditioned on the updated embeddings from previous levels.

B.4. Pre-training

Before optimizing for specific molecular properties, we initialize the policy to capture the fundamental syntax of stable chemistry. We utilize the ChEMBL database (Davies et al., 2015) (version 35) as a source of chemically valid structures. Following the pre-training protocol of GraphXForm (Pirnay et al., 2025), we filtered the database to include only molecules

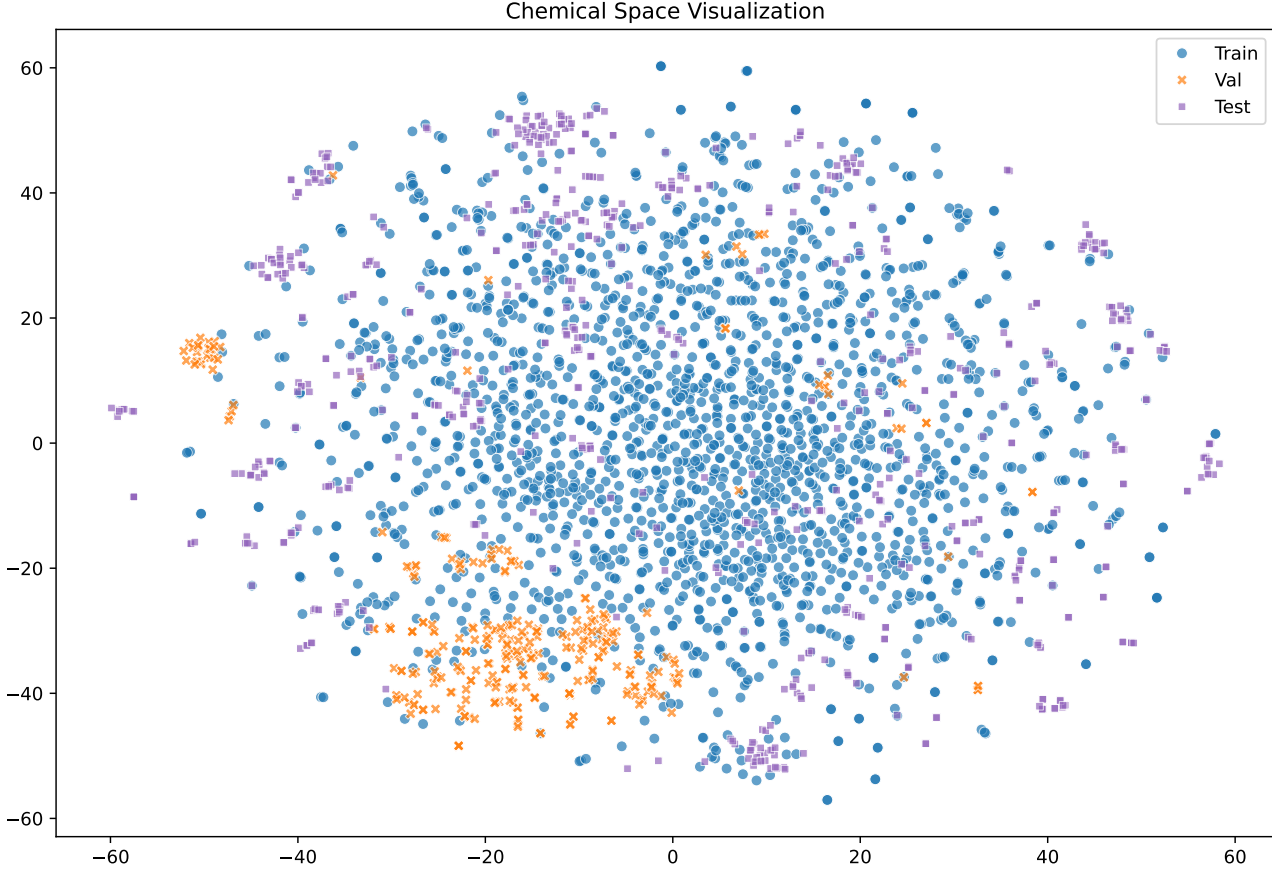


Figure 5. Structural Generalization Split. t-SNE visualization of the chemical space (Morgan Fingerprints) for Training, Validation, and Test scaffolds. The cluster-based splitting strategy ensures that Test scaffolds (purple) occupy distinct regions of chemical space compared to the Training set (blue) and Validation set (orange), enforcing a test of out-of-distribution generalization.

composed of atoms within our defined alphabet. This resulted in a training set of approximately 1.5 million molecules and a validation set of roughly 70,000 molecules. Pre-training was performed with a batch size of 512 and dropout rate of 0.1, over 1.5 million batches in total.

Since our policy π_θ operates sequentially, we cannot train on static graphs directly. Instead, we transform each molecule $G \in \mathcal{D}_{pre}$ into a dynamic construction trajectory. We define a mapping function $\Phi : G \rightarrow \tau^*$ that decomposes the graph into a sequence of ground-truth actions $\tau^* = (a_0^*, s_1, a_1^*, \dots, a_T^*)$ which reconstructs G atom-by-atom starting from a single node (e.g., a carbon atom). While multiple valid action permutations often exist for a single graph (e.g., different traversal orders), we select a canonical decomposition to serve as the fixed supervised label for training.

We then treat these trajectories as expert demonstrations. The policy is trained via standard supervised learning (teacher forcing) to minimize the cross-entropy loss between the predicted action distribution and the ground-truth action a_t^* at each step t :

$$\mathcal{L}_{MLE}(\theta) = -\mathbb{E}_{G \sim \mathcal{D}_{pre}} \left[\sum_{t=0}^T \log \pi_\theta(a_t^* | s_t^*) \right] \quad (6)$$

where s_t^* is the partial graph state resulting from the ground-truth prefix $a_{0:t-1}^*$. This ensures the policy generates chemically plausible structures before optimization begins.

Table 4. Performance comparison of GRXForm (Ours) against state-of-the-art baselines on goal-directed generation tasks (PMO benchmark). Results report the mean and standard deviation of the top-10 AUC, over 3 to 5 independent runs (details in Appendix D). The top three results for each task are colored in **blue** (1st), **orange** (2nd), and **green** (3rd).

TASK	GRXFORM (OURS)	GENMOL	SYNGBO	F-RAG	GENETIC GFN	MOL GA	REINVENT	GP BO
ALBUTEROL SIMILARITY	0.970 \pm 0.006	0.937 \pm 0.010	0.947 \pm 0.024	0.977 \pm 0.002	0.949 \pm 0.010	0.928 \pm 0.015	0.881 \pm 0.016	0.964 \pm 0.050
AMLODIPINE MPO	0.666 \pm 0.021	0.810 \pm 0.012	0.670 \pm 0.088	0.749 \pm 0.019	0.761 \pm 0.019	0.740 \pm 0.055	0.644 \pm 0.019	0.720 \pm 0.061
CELECOXIB REDISCOVERY	0.862 \pm 0.006	0.826 \pm 0.018	0.856 \pm 0.013	0.778 \pm 0.007	0.802 \pm 0.029	0.629 \pm 0.062	0.717 \pm 0.027	0.573 \pm 0.019
DECO HOP	0.944 \pm 0.026	0.960 \pm 0.010	0.831 \pm 0.039	0.936 \pm 0.011	0.733 \pm 0.109	0.656 \pm 0.013	0.662 \pm 0.044	0.672 \pm 0.118
DRD2	0.991 \pm 0.001	0.995 \pm 0.000	0.981 \pm 0.010	0.992 \pm 0.000	0.974 \pm 0.006	0.950 \pm 0.004	0.957 \pm 0.007	0.902 \pm 0.117
FEXOFENADINE MPO	0.829 \pm 0.027	0.894 \pm 0.028	0.833 \pm 0.018	0.856 \pm 0.016	0.856 \pm 0.039	0.835 \pm 0.012	0.781 \pm 0.013	0.806 \pm 0.006
GSK3 β	0.928 \pm 0.005	0.986 \pm 0.003	0.924 \pm 0.027	0.969 \pm 0.003	0.881 \pm 0.042	0.894 \pm 0.025	0.885 \pm 0.031	0.877 \pm 0.055
ISOMERS C7H8N2O2	0.962 \pm 0.002	0.942 \pm 0.004	0.975 \pm 0.006	0.955 \pm 0.008	0.969 \pm 0.003	0.926 \pm 0.014	0.942 \pm 0.012	0.911 \pm 0.031
ISOMERS C9H10N2O2PF2CL	0.795 \pm 0.038	0.833 \pm 0.014	0.875 \pm 0.013	0.850 \pm 0.005	0.897 \pm 0.007	0.894 \pm 0.005	0.838 \pm 0.030	0.828 \pm 0.126
JNK3	0.914 \pm 0.037	0.906 \pm 0.023	0.910 \pm 0.021	0.904 \pm 0.004	0.764 \pm 0.069	0.835 \pm 0.040	0.782 \pm 0.029	0.785 \pm 0.072
MEDIAN 1	0.358 \pm 0.028	0.398 \pm 0.000	0.357 \pm 0.001	0.340 \pm 0.007	0.379 \pm 0.010	0.329 \pm 0.006	0.363 \pm 0.011	0.408 \pm 0.003
MEDIAN 2	0.277 \pm 0.024	0.359 \pm 0.004	0.349 \pm 0.001	0.323 \pm 0.005	0.294 \pm 0.007	0.284 \pm 0.035	0.281 \pm 0.002	0.349 \pm 0.001
MESTRANOL SIMILARITY	0.954 \pm 0.015	0.982 \pm 0.000	0.759 \pm 0.023	0.671 \pm 0.021	0.708 \pm 0.057	0.762 \pm 0.048	0.634 \pm 0.042	0.930 \pm 0.106
OSIMERTINIB MPO	0.848 \pm 0.011	0.876 \pm 0.008	0.856 \pm 0.024	0.866 \pm 0.009	0.860 \pm 0.008	0.853 \pm 0.005	0.834 \pm 0.010	0.833 \pm 0.011
PERINDOPRIL MPO	0.569 \pm 0.046	0.718 \pm 0.012	0.774 \pm 0.006	0.681 \pm 0.017	0.595 \pm 0.014	0.610 \pm 0.038	0.535 \pm 0.015	0.651 \pm 0.030
QED	0.942 \pm 0.000	0.942 \pm 0.000	0.940 \pm 0.002	0.939 \pm 0.001	0.942 \pm 0.000	0.941 \pm 0.001	0.941 \pm 0.000	0.947 \pm 0.000
RANOLAZINE MPO	0.833 \pm 0.012	0.821 \pm 0.011	0.839 \pm 0.016	0.820 \pm 0.016	0.819 \pm 0.018	0.830 \pm 0.010	0.770 \pm 0.005	0.810 \pm 0.011
SCAFFOLD HOP	0.588 \pm 0.030	0.628 \pm 0.008	0.541 \pm 0.008	0.576 \pm 0.014	0.615 \pm 0.100	0.568 \pm 0.017	0.551 \pm 0.024	0.529 \pm 0.020
SITAGLIPTIN MPO	0.513 \pm 0.074	0.584 \pm 0.034	0.454 \pm 0.074	0.601 \pm 0.011	0.634 \pm 0.039	0.677 \pm 0.055	0.470 \pm 0.041	0.474 \pm 0.085
THIOTHIXENE REDISCOVERY	0.691 \pm 0.106	0.692 \pm 0.123	0.647 \pm 0.003	0.584 \pm 0.009	0.583 \pm 0.034	0.544 \pm 0.067	0.544 \pm 0.026	0.727 \pm 0.089
TROGLITAZONE REDISCOVERY	0.504 \pm 0.023	0.867 \pm 0.022	0.579 \pm 0.002	0.448 \pm 0.017	0.511 \pm 0.054	0.487 \pm 0.024	0.458 \pm 0.018	0.756 \pm 0.141
ZALEPLON MPO	0.495 \pm 0.008	0.584 \pm 0.011	0.529 \pm 0.017	0.486 \pm 0.004	0.552 \pm 0.033	0.514 \pm 0.033	0.533 \pm 0.009	0.499 \pm 0.025
SUM	16.433	17.540	16.426	16.301	16.078	15.686	15.003	16.304

C. Dataset Preparation and Scaffold Splitting

To evaluate the generalization capability of the model, we utilized the ZINC-250k dataset (Sterling & Irwin, 2015). A rigorous cluster-based split was implemented to ensure that the test set consists of topologically distinct scaffolds rather than local structural variations.

We performed Murcko scaffold decomposition using RDKit (Landrum, 2006) and clustered the resulting scaffolds using the Butina algorithm (Butina, 1999) on Morgan fingerprints (radius 2, 2048 bits) with a Tanimoto similarity cutoff of 0.4. Entire clusters were assigned to training, validation, or testing, reserving 500 structurally distinct scaffolds for the test set.

Figure 5 visualizes the chemical space of the resulting splits. The clear separation between training (blue) and test (red) distributions confirms that the model must learn to generalize optimization rules to unseen regions of chemical space rather than memorizing training examples.

D. PMO Benchmark

To adhere to the PMO instance optimization protocol, we run GRXForm using online reinforcement learning. As we implement *de-novo* generation by initializing every episode with a single carbon atom, there is no variation in starting states. Consequently, the group-relative advantage formulation is not required; we therefore fine-tune the policy using standard REINFORCE with a global baseline.

Entropy Regularization. To prevent premature convergence and encourage exploration, we augment the objective with an entropy regularization term. We calculate the entropy $H(\pi_\theta(\cdot|s_t))$ of the policy distribution at each step t . To ensure numerical stability and validity, we strictly compute this over valid actions by filtering out tokens masked by the valence constraints:

$$H(\pi_\theta(\cdot|s_t)) = - \sum_{k \in \mathcal{A}_{valid}} \pi_\theta(a_k|s_t) \log \pi_\theta(a_k|s_t) \quad (7)$$

where \mathcal{A}_{valid} is the set of chemically valid actions at state s_t .

The final gradient update is performed by maximizing the joint objective $\mathcal{J}_{total} = \mathcal{J}_{RL} + \beta H$. Since sampling trajectories is inexpensive compared to parameter updates, we perform a single gradient update per batch using the following estimator:

$$\nabla_\theta \mathcal{J}(\theta) \approx \frac{1}{BG} \sum_{i=1}^B \sum_{j=1}^G \left[A_{i,j} \sum_{t=1}^{T_{i,j}} \nabla_\theta \log \pi_\theta(a_t|s_{<t}) + \beta \sum_{t=1}^{T_{i,j}} \nabla_\theta H(\pi_\theta(\cdot|s_{<t})) \right] \quad (8)$$

Here, $A_{i,j}$ is the advantage calculated against the global moving average baseline, and β is the task-specific entropy coefficient.

Hyperparameters. Table 5 details the specific entropy coefficient (β) used for each task in the PMO benchmark. We found that while many tasks converged stably with $\beta = 0$, certain optimization landscapes benefited from small regularization values ($\beta \in \{0.001, 0.002\}$).

Table 5. Entropy coefficients (β) used for GRXForm across PMO Benchmark tasks.

PMO Task	Entropy Coeff. (β)
Albuterol Similarity	0.002
Amlodipine MPO	0.0
Celecoxib Rediscovery	0.001
Deco Hop	0.0
DRD2	0.0
Fexofenadine MPO	0.0
GSK3 β	0.001
Isomers C7H8N2O2	0.002
Isomers C9H10N2O2PF2Cl	0.0
JNK3	0.0
Median 1	0.001
Median 2	0.0
Mestranol Similarity	0.001
Osimertinib MPO	0.0
Perindopril MPO	0.001
QED	0.001
Ranolazine MPO	0.0
Scaffold Hop	0.0
Sitagliptin MPO	0.0
Thiothixene Rediscovery	0.001
Troglitazone Rediscovery	0.0
Zaleplon MPO	0.001

The benchmark evaluates sample efficiency using the Area Under the Curve (AUC) of the top-10 property scores, calculated via the trapezoidal rule at intervals of 100 oracle calls. This metric plots the average score of the top-10 molecules found so far (y -axis) against the number of oracle calls (x -axis) consumed during the online training trajectory. By integrating this curve, the metric penalizes methods that require a long warm-up period or extensive exploration to find their first high-scoring candidates. A high AUC indicates that the agent rapidly locates high-scoring molecules early in the learning process.

We compare GRXForm against state-of-the-art baselines reported in Lee et al. (2025) and Lo et al. (2025). These baselines encompass discrete diffusion (GenMol), synthesis-aware optimization (SynGBO), retrieval-augmented generation (f-RAG), evolutionary and flow-based strategies (Genetic GFN, Mol GA), reinforcement learning (REINVENT), and Bayesian Optimization (GP BO). We report results averaged over 3 independent runs for GRXForm. This follows the precedent set by recent state-of-the-art methods, such as GenMol (Lee et al., 2025) and f-RAG (Lee et al., 2024), which also report performance over 3 independent runs. Baseline results for SynGBO (Lo et al., 2025), Genetic GFN, Mol GA, REINVENT, and GP BO are reported over 5 independent runs, as sourced from Lo et al. (2025).

Task Exclusion. We evaluate on 22 of the 23 standard PMO tasks, excluding the *Valsartan SMARTS* task. While this task was originally included in the benchmark to assess hard constraint satisfaction (i.e., the ability to generate a molecule containing a specific required substructure), we find it ill-suited for benchmarking optimization efficiency. The task requires the generated molecule to contain the substructure CN(C=O)Cc1ccc(c2cccc2)cc1 to receive non-zero feedback. Unlike other tasks that offer more intermediate signals, this requirement creates a cliff-like landscape where the reward is strictly zero until the exact motif is present.

While recent methods such as GenMol and f-RAG achieve high scores on this task, we posit that this performance likely reflects the robust generative priors learned from their billion-scale pretraining on the SAFE dataset (Noutahi et al., 2024) rather than optimization efficiency. The SAFE dataset aggregates molecules from both ZINC and UniChem, effectively covering a vast space of known pharmaceutical compounds. Such extensive pretraining could allow these models to propose complex drug-like scaffolds directly from their learned distribution, potentially bypassing the need to navigate the reward landscape. In contrast, for algorithms that rely on traversing the chemical space via feedback signals, the lack of intermediate guidance makes this task chemically unnavigable. Therefore, we exclude it to isolate and evaluate the search capability of the algorithms rather than their capacity for constraint satisfaction or memorization.

E. Oracle Complexity and Amortization Analysis

A defining characteristic of amortized optimization is the decoupling of expensive oracle evaluations (e.g., docking simulations) from the inference phase. By shifting the computational burden to a one-time training period, the marginal cost of generating optimized molecules becomes negligible. In Table 6, we contrast the fixed training budget of amortized policies against the linear cost scaling of instance-specific optimizers.

Table 6. Oracle Consumption Analysis. For amortized models, values denote the *fixed cumulative* calls required to train the policy. For instance optimizers, values denote the *average* calls required to optimize a single scaffold.

TYPE	METHOD	TRAINING COST (FIXED TOTAL)	INFERENCE COST (PER INSTANCE)
AMORTIZED	GRXFORM (OURS)	$\approx 50,000$	0
	GRAPHXFORM (TASAR)	280,000	0
	DRUGEX v3	640,000	0
INSTANCE	MOL GA	N/A	$\approx 10,000$ (MAX)
	GENMOL	N/A	≈ 200

We define the amortization break-even point as the threshold where the cumulative cost of instance optimization exceeds the fixed training budget of GRXForm ($\approx 50,000$ calls). For sample-intensive baselines like Mol GA (up to 10^4 calls per task), parity is reached after just **5 scaffolds**. For deep generative models with higher sample efficiency, such as GenMol (≈ 200 calls per task), the break-even point is **250 scaffolds**.

Beyond oracle counts, wall-clock latency presents a significant bottleneck. GenMol required approximately 7 minutes to complete the necessary 10 generations for convergence, whereas GRXForm can perform inference in milliseconds per input structure with batching. This latency difference renders iterative deep generative search computationally expensive for large-scale library design. All timing benchmarks were conducted on a machine with a single NVIDIA H100 GPU and Intel Xeon 8468 Sapphire (2.1 GHz, 24 cores usable).

F. Hyperparameters and Configuration

F.1. GRXForm Implementation Details

This appendix details the network architecture, optimization settings, and hyperparameters used for the GRXForm experiments, covering both the De Novo and Scaffold-constrained (GRPO and REINFORCE) settings, as well as the original GraphXForm baseline.

F.1.1. NETWORK ARCHITECTURE AND OPTIMIZATION

Table 7 summarizes the global hyperparameters used across all experiments for the Transformer-based policy and the optimization process. For all GRXForm experiments, we restrict the maximum number of atoms in a generated molecule to 50.

F.1.2. EXPERIMENT-SPECIFIC CONFIGURATIONS

Table 8 outlines the differences between GRXForm-DeNovo, GRXForm-REINFORCE, GRXForm-GRPO, and the GraphXForm baseline.

Table 7. Global Network Architecture and Optimization Hyperparameters.

Parameter	Value
<i>Network Architecture</i>	
Latent Dimension	512
Number of Transformer Blocks	10
Number of Attention Heads	16
<i>Optimization (ADAM)</i>	
Learning Rate	1×10^{-4}
Weight Decay	0
Gradient Clipping (L2-norm)	1.0
LR Schedule Decay Factor	1.0 (Constant)
<i>Reinforcement Learning (GRPO)</i>	
GRPO Updates per Epoch	1
Entropy Coefficient β	0.0

Baseline Note: The **GraphXForm** column represents the original GraphXForm training methodology (Pirnay et al., 2025). Unlike our RL-based approach, this baseline is trained via self-improvement learning to mimic high-scoring trajectories discovered by the *Take a Step and Reconsider* (TASAR) (Pirnay & Grimm, 2024b) search heuristic. It serves as a direct comparison between RL and search-based imitation learning. We utilize the default hyperparameters for GraphXForm, modifying only the beam width to ensure consistency with our other experiments.

Table 8. Experiment-Specific Hyperparameters. All experiments were capped at a global budget of 50,000 oracle calls.

	GRXForm- DeNovo	GRXForm- REINFORCE	GRXForm- GRPO	GraphXForm
Objective	Kinase MPO	Kinase MPO	Kinase MPO	Kinase MPO
Initialization	Single Carbon	Scaffolds + C [‡]	Scaffolds + C [‡]	Single Carbon
Method	Dr. GRPO	REINFORCE [*]	Dr. GRPO	TASAR (SIL)
Grouping	N/A	False	True	N/A
Starting Structures / Epoch	1	10	10	1
Beam Width	160	16	16	160
Total Batch Size	≈ 160	$\approx 160 (16 \times 10)$	$\approx 160 (16 \times 10)$	N/A [†]
Max Epochs	500	500	500	500

^{*}Implemented as GRPO without grouping (Global Baseline).

[†]GraphXForm utilizes elite replay buffer imitation learning; parameter updates are performed on state-action pairs sampled from a cumulative buffer of top molecules rather than an on-policy batch.

[‡]In each epoch, the model is initialized with 1 single carbon atom and 9 scaffolds randomly sampled from the library.

Prodrug Objective Settings For the *Prodrug* experiments (not listed in Table 8), the configuration followed the GRXForm-GRPO setup but utilized **4 specific parent molecules** as starting points. Consequently, the sampling beam width was set to 32 per parent, resulting in an effective total batch size of $32 \times 4 = 128$ trajectories per epoch.

F.2. LibINVENT Implementation Details

We utilized the official LibINVENT implementation from Reinvent (Loeffler et al., 2024). During experimentation, we encountered severe memory limitations (Out of Memory on an 80GB H100 GPU) when scaling the model beyond a small batch of unique scaffolds. Consequently, we restricted its training to 8 randomly sampled scaffolds as that was around the maximum before most runs encountered out of memory issues.

Furthermore, LibINVENT requires the manual specification of attachment points and supports only one active growing vector per input SMILES string. This contrasts with GRXForm, which autonomously identifies and utilizes multiple attachment points simultaneously. To ensure a fair comparison, we pre-processed the data to create an expanded dataset:

for every unique scaffold, we generated multiple entries, each with a single attachment point (*) placed at a different valid modification site. This allowed the model to attempt decoration at all potential positions. During evaluation, we aggregated the results for each core scaffold and reported the metrics corresponding to the best-scoring derivative found across all expanded attachment points.

The key training hyperparameters used for the Kinase MPO task are:

- **General Parameters:** Batch size = 64; Randomize SMILES = True.
- **Learning Strategy:** Type = DAP (Diversity Augmented Policy); $\sigma = 128$ (Balances score vs. prior); Learning rate = 10^{-4} .
- **Diversity Filter:** Type = IdenticalMurckoScaffold; Bucket size = 25; Min score = 0.4; Min similarity = 0.4.
- **Training Budget:** Max steps = 3000.

F.3. DrugEx v3 Implementation Details

We utilized the official DrugEx v3 implementation (Liu et al., 2023), specifically the Graph Transformer architecture. We initialized the policy using the official pre-trained checkpoint DrugEx_PT_ChEMBL27, which was trained on the ChEMBL 27 dataset to learn general chemical validity.

For the optimization phase, we employed the `FragGraphExplorer`, which fine-tunes the agent using a Reinforcement Learning framework. To maintain diversity and regularization, a frozen copy of the pre-trained model is used as a “mutation” network. The multi-objective reward signal is handled via Pareto Crowding Distance sorting.

The key training hyperparameters used in our experiments are:

- **General Parameters:** Batch size = 64; Exploration rate (ϵ) = 0.1.
- **Training Budget:** Max epochs = 500.
- **Exploration Settings:**
 - `n_samples` = 500 (Number of samples generated per epoch for update).
 - `beta` = 0.0 (Reward baseline coefficient).
 - `no_multifrag_smiles` = True (Ensures generation of single connected components).
- **Reward Scheme:** Pareto Crowding Distance.
- **Scoring Modifiers:** Raw oracle scores were processed via `ClippedScore` modifiers to ensure stable gradients (GSK3 β /JNK3: [0.3, 0.5], QED: [0.4, 0.6], SA: [0.5, 0.67]).

F.4. GenMol Implementation Details

We utilized the official GenMol implementation (Lee et al., 2025) in its scaffold decoration mode. To ensure consistent performance, we adhered to the authors’ recommended default configuration for structural elaboration tasks.

A key limitation of GenMol in structurally constrained design is its requirement for explicit tokens to designate attachment points at each optimization iteration. This typically necessitates manual user intervention. To adapt the model for our automated benchmark, we implemented a heuristic that automatically places up to 3 random attachment points ([*]) on the scaffold at each step, allowing the model to perform autonomous optimization without a human-in-the-loop.

The key hyperparameters used are:

- **Sampling Parameters:** Softmax temperature = 1.5; Randomness = 2; Gamma (γ) = 0.3.
- **Generation Constraints:** Minimum added length (`min_add_len`) = 24.
- **Attachment Heuristic:** Random placement of up to 3 attachment tokens per iteration to enable fully automated scaffold decoration.
- **Population Settings:** `NUM_GENERATIONS` = 10; `NUM_SAMPLES` = 32. We observed that the population fitness scores plateaued within 10 generations, indicating that further iterations yielded negligible gains at the cost of significant additional compute.

F.5. Mol GA Implementation Details

We utilized the default hyperparameters provided by the `mol_ga` framework for our genetic algorithm implementation. The core configuration consisted of a population size of 10,000 molecules evolving over 100 generations, with an offspring size of 1,000 per generation.

Fitness Function Modification: We modified the fitness function to act as a hard constraint: offspring that violate the scaffold substructure requirement are assigned a zero score, forcing the genetic algorithm to prioritize structure preservation.

For reproducibility, the specific default hyperparameters and mutation probabilities used in this study are detailed in Table 9; we have not modified these from the defaults in the code.

Table 9. Hyperparameters and configuration details for Mol GA.

Parameter	Value
<i>General GA Settings</i>	
Population Size	10,000
Offspring Size	1,000
Max Generations	100
Selection Strategy	Greedy (Top-N)
Parent Sampling Strategy	Uniform Quantile Sampling (25 quantiles)
Mating Pool Size	2,000
<i>Offspring Generation Strategy</i>	
Crossover Fraction	0.90
Mutation-Only Fraction	0.10
Post-Crossover Mutation Rate	0.01
Crossover Type	50% Ring / 50% Non-Ring
<i>Graph Mutation Probabilities</i>	
Insert Atom	0.15
Append Atom	0.15
Change Bond Order	0.14
Delete Cyclic Bond	0.14
Add Ring	0.14
Delete Atom	0.14
Change Atom Type	0.14